



Sensitivity analysis of the 1-D SFR thermal stratification model via discrete adjoint sensitivity method

Cihang Lu, Zeyun Wu*

Department of Mechanical and Nuclear Engineering, Virginia Commonwealth University, 401 W. Main St., Richmond, VA 23219, United States

ARTICLE INFO

Keywords:

Adjoint sensitivity analysis
Forward sensitivity analysis
Thermal stratification
Sodium-cooled fast reactor

ABSTRACT

This paper presents a parameter sensitivity analysis on a thermal stratification (TS) model by using the discrete sensitivity method. The TS model was recently developed in our research group to efficiently predict the TS phenomenon in pool-type Sodium-cooled Fast Reactors. The fluid temperature gradient was considered as the figure of merit in the sensitivity analysis because it best characterizes the thermal stratification phenomenon. The sensitivities of the fluid temperature gradient with respect to four different parameters were investigated, including jet volumetric flow rate Q_{jet} , jet temperature T_{jet} , heat capacity of the ambient fluid $C_{p,amb}$, and static thermal conductivity of the ambient fluid $k_{c,amb}$. The sensitivity analysis was conducted through both the conventional forward sensitivity method and the advanced adjoint sensitivity method, which is more effective in cases where the number of outputs is small and the number of input parameters is large.

The sensitivities obtained in this study suggested that perturbations in Q_{jet} , $C_{p,amb}$, and $k_{c,amb}$ could introduce either positive or negative changes to the temperature gradient, depending on the axial location and the elapsed time of the experiment. However, an increase in T_{jet} always decreased the temperature gradient. Moreover, the impact of T_{jet} on the maximum temperature gradient was several times higher than that of the other three parameters, which indicated that additional attention may need to be paid to the occurrence of thermal stratification in the sodium pool when the impinging jet has a large temperature change. This study also provides a step-by-step example for the application of the discrete adjoint sensitivity method to the time-dependent nonlinear systems.

1. Introduction

Thermal stratification (TS) is a thermal-fluid phenomenon that needs to be considered in nuclear reactor designs. When it occurs in the hot plenum of a pool-type liquid-metal-cooled reactor, for example, thermal stratification causes the formation of thermal-stratified layers of the coolant with a large vertical temperature gradient, which further introduce large uncertainties to the reactor safety (Wu et al., 2020). In this regard, a fast-running one-dimensional (1-D) model was recently developed in our research group to predict the thermal stratification phenomenon in pool-type Sodium-cooled Fast Reactors (SFRs). The 1-D model had similar performance with CFD calculations in terms of the prediction of thermal stratification, while the computational cost was on the order of seconds by using a single processor core (Lu et al., 2020a, 2020b, 2020c).

In order to prevent the thermal stratification and mitigate the damage it may cause, the key parameters associated with this phenomenon are worthy of investigation. The intention of this study is to identify the

factors that impact the severity of the thermal-stratification phenomenon the most to inform safety analysts with these TS sensitive parameters. For this purpose, we investigated the sensitivity of the temperature gradient, which best characterizes the thermal stratification phenomenon, to different parameters by using the 1-D thermal stratification model. We employed both the conventional forward sensitivity method and the advanced adjoint sensitivity method to perform the sensitivity analysis in this work. Compared with the conventional forward method, the adjoint method is more efficient for the computation of sensitivity derivatives in cases when the number of outputs is small and the number of input parameters is large (Wang, 2013).

The adjoint sensitivity method has been widely used in different research fields, including meteorology (Errico, 1997; Rocklin and Constantinescu, 2009) and electricity generation (Son and Lee, 2018). This method has also been frequently employed in aerodynamics for the modeling of design sensitivities (Thomas et al., 2005; Zahr et al., 2016), which were further used for the optimization of both airfoil shape (Nadarajah and Jameson, 2002; Nadarajah, 2003; Mani and Mavriplis,

* Corresponding author.

E-mail address: zwu@vcu.edu (Z. Wu).

2008; Rumpfkeil and Zingg, 2010; Mishra et al., 2015; Thomas and Dowell, 2019) and angle of attack (Giles et al., 2003), in order to get a maximized lift and a minimized drag. Cacuci and others introduced the adjoint sensitivity method to the nuclear engineering field in the early 1980's (Cacuci et al., 1980; Cacuci, 1981a, 1981b; Cacuci and Wacholder, 1982), and this method has been frequently employed in nuclear engineering since then (Drzewiecki, 2013; Hu, 2018). The adjoint sensitivity method can generally be categorized into two types, the continuous adjoint sensitivity method and the discrete adjoint sensitivity method. When the continuous adjoint sensitivity method is employed, the adjoint equations will be derived analytically from the governing forward equations, and then solved either analytically or numerically through standard discretization methods. When the discrete adjoint sensitivity method is employed, the governing forward equations will first be discretized and the adjoint equations will then be derived and computed in the discretized form (Duffy, 2009). The two methods were compared in different works, but no clear conclusions on which one is better were obtained (Li and Petzold, 2004; B. G. van Bloemen Waanders et al., "Sensitivity technologies for large scale simulation," Technical report, Sandia national laboratory, SAND, 2005; Hu and Kozlowski, 2019). Both methods have been applied to nuclear engineering problems, and some examples are given as follows. Cacuci et al. (1980) applied both the continuous and the adjoint sensitivity methods to a transient nonlinear reactor thermal-hydraulic problem. They investigated the sensitivities of various figures of merit, including peak fuel temperature, peak cladding temperature, and peak outlet coolant temperature, etc., and demonstrated the results from both approaches to be equivalent. Cacuci et al. (2016) applied the continuous adjoint method to a heat transport benchmark problem, where the steady-state radial conduction in a fuel rod and the axial heat convection in a coolant flowing along the rod were considered. By employing the continuous adjoint method, they gave the exact analytical solutions to the sensitivities of the fuel temperature and the coolant temperature. Cacuci and Ionescu-Bujor (Cacuci and Ionescu-Bujor, 2000; Ionescu-Bujor and Cacuci, 2000) applied both the continuous and adjoint sensitivity methods to nonequilibrium, nonhomogeneous two-fluid-flow problems. Both boron concentration and noncondensable gases were considered, and the implementation of the adjoint methods in the system-level thermal-hydraulic code, RELAP5/MOD3.2, was presented.

In this work, we adopted the discrete adjoint sensitivity method because the discrete form of the 1-D thermal stratification model was readily available. Moreover, step-by-step applications of the discrete adjoint sensitivity method to time-dependent nonlinear systems were rarely provided in the existing literature. This paper can therefore serve as a detailed example for the use of the discrete adjoint sensitivity method, in order to facilitate the learning curve of this method for those incoming researchers who are interested in this concept. The rest of the paper is organized as follows: Section 2 briefly discusses the derivation of the adjoint sensitivity method. Section 3 presents a step-by-step application of the discrete adjoint sensitivity method to the 1-D thermal stratification model. Section 4 verifies the results calculated by the adjoint sensitivity method against that obtained through the forward method, and provides further sensitivity analysis by using the adjoint sensitivity method. Section 5 concludes this work by summarizing the conclusions drawn from the sensitivity analysis.

2. The discrete adjoint sensitivity method

Detailed derivations of the adjoint systems have been presented in the literature (Mishra et al., 2015; Cacuci, 1981; Hu and Kozlowski, 2019; Cao et al., 2003). The derivation is briefly presented again in this section such that the application of the discrete adjoint method to the 1-D thermal stratification model, which will be detailed in the next section, can be more straightforward.

Considering a generic nonlinear system governed by the state equation in a residual form

$$F(x, \theta) = 0 \quad (1)$$

x is considered as the state variable that needs to be solved, and θ is the system parameter variable on which x is dependent. A general response variable $J(x)$, which is literally dependent only on x , is assumed. In theory, there are two distinguished approaches for calculating the sensitivity of response variable $J(x)$ to the system parameter θ , which essentially need to compute the variation of the response $\delta J(x)$. The first approach is through the well-understood "forward sensitivity method" by expressing $\delta J(x)$ as

$$\delta J(x) = \frac{dJ(x)}{dx} \frac{dx}{d\theta} \delta\theta \quad (2)$$

where δ is the variation operator. The "forward sensitivity method" is theoretically straightforward, but the calculation of $\frac{dx}{d\theta}$ requires repetitive computations of the forward model. This method becomes expensive if the dimension of θ is large. The second sensitivity analysis approach is through the so-called "adjoint sensitivity method", which starts by expressing $\delta J(x)$ as

$$\delta J(x) = \frac{dJ(x)}{dx} \delta x \quad (3)$$

and then manages to evaluate the $\delta J(x)$ by precluding the calculation of the state variable variation δx .

From Eq. (1), we have

$$\delta F(x, \theta) = \frac{\partial F(x, \theta)}{\partial x} \delta x + \frac{\partial F(x, \theta)}{\partial \theta} \delta\theta = 0 \quad (4)$$

By introducing the vector of Lagrangian multipliers, Φ^T , Eq. (3) can also be written as

$$\delta J(x) = \frac{dJ(x)}{dx} \delta x + \Phi^T \left(\frac{\partial F(x, \theta)}{\partial x} \delta x + \frac{\partial F(x, \theta)}{\partial \theta} \delta\theta \right) \quad (5)$$

In order to cancel out the term δx (which is the goal of the derivation), we must have

$$\frac{dJ(x)}{dx} + \Phi^T \frac{\partial F(x, \theta)}{\partial x} = 0 \quad (6)$$

Eq. (6) is sometimes referred to as the "adjoint equation" of the forward model [i.e., Eq. (1)], and Φ is referred to as the adjoint solution. With Eq. (6), Eq. (5) is reduced to

$$\delta J(x) = \Phi^T \frac{\partial F(x, \theta)}{\partial \theta} \delta\theta \quad (7)$$

By representing Φ^T with a direct matrix inversion from Eq. (6), Eq. (7) can be further expressed as a function of $\delta\theta$,

$$\delta J(x) = -\frac{dJ(x)}{dx} \left(\frac{\partial F(x, \theta)}{\partial x} \right)^{-1} \frac{\partial F(x, \theta)}{\partial \theta} \delta\theta \quad (8)$$

Eq. (8) is the starting point of the discrete adjoint sensitivity analysis. As can be seen, to enable an adjoint sensitivity calculation, one is required to compute three terms, $\frac{dJ(x)}{dx}$, $\left(\frac{\partial F(x, \theta)}{\partial x} \right)^{-1}$, and $\frac{\partial F(x, \theta)}{\partial \theta}$. A detailed procedure on the computation of these three terms for a specific problem of interest (i.e., the thermal stratification model) is outlined in Section 3.3.

3. Discrete adjoint sensitivity analysis to the 1-D thermal stratification model

This section presents a step-by-step application of the discrete adjoint sensitivity method to the 1-D thermal stratification model. A brief introduction of the 1-D thermal stratification model and its discretization is provided in Section 3.1, while the experiment, to which the discrete adjoint sensitivity method was applied, is described in Section

3.2. The inclusion of these two subsections should make the application of the discrete adjoint sensitivity method, illustrated in Section 3.3, more straightforward.

3.1. 1-D thermal stratification model

A fast-running 1-D model was recently developed in our research group (Lu et al., 2020a, 2020b, 2020c) to predict the thermal stratification phenomenon in SFRs, the essence of which was to use integral techniques to convert the jets to source terms in the diffusion convection equation. By combining the equations of conservation of mass and energy,

$$\begin{aligned} & \rho_{amb} c_{p,amb} \frac{\partial T_{amb}}{\partial t} + \rho_{amb} c_{p,amb} \frac{Q_{jet}}{A_{amb}} \frac{\partial T_{amb}}{\partial z} - \frac{\partial}{\partial z} \left(k_{amb} \frac{\partial T_{amb}}{\partial z} \right) \\ & = \frac{c_{p,jet} \rho_{jet}}{A_{amb}} Q_{jet} (T_{jet} - T_{amb}) \end{aligned} \quad (9)$$

was obtained as the resultant governing equation, which can be solved for the temperature profile of the ambient fluid at different time steps. In this equation, ρ_{amb} , $c_{p,amb}$, k_{amb} , A_{amb} , and T_{amb} represent respectively the mass density, heat capacity, effective thermal conductivity, cross-sectional area, and temperature of the ambient fluid. ρ_{jet} , $c_{p,jet}$, Q_{jet} , and T_{jet} represent respectively the mass density, heat capacity, volumetric flow rate, and the temperature of the impinging jet. Q_{jet} is the linear volumetric dispersion rate of the impinging jet.

In order to solve Eq. (9) numerically, standard staggered scheme with uniform mesh size was used for the spatial discretization, and semi-implicit approach was used for the temporal discretization. The upwind scheme was used to approximate the first order spatial derivatives, while the center difference scheme was used to approximate the second order spatial derivatives. The discretized form of Eq. (9) for the mesh-average temperature of the ambient fluid at the mesh n and at the time step m can be written as

$$\begin{aligned} & \rho_n^{m-1} c_{p,n}^{m-1} \frac{T_n^m - T_n^{m-1}}{\Delta t} + \rho_n^{m-1} c_{p,n}^{m-1} u_{z,n} \frac{T_n^m - T_n^{m-1}}{\Delta z} - \frac{2}{\Delta z} k_n^{m-1} \left(\frac{T_{n+1}^m - T_n^m}{2\Delta z} - \frac{T_n^m - T_{n-1}^m}{2\Delta z} \right) \\ & = \frac{1}{A_{amb,n}} c_{p,jet} \rho_{jet} Q_{jet,n} (T_{jet} - T_n^{m-1}) \end{aligned} \quad (10)$$

where $A_{amb,n}$ represents the cross-sectional area of the ambient fluid at mesh n , and $u_{z,n}$ represents the corresponding rising velocity of the ambient fluid. All the thermal-hydraulic parameters utilized in Eq. (10) were calculated in the previous time step. A system of $(M+1) \times N$ algebraic equations, F , can be established for the ambient fluid temperature predictions, T . By solving F , the ambient fluid temperature can be calculated at N spatial steps and $(M+1)$ time steps, which consist of M time steps to be predicted and the initial condition. We can note

$$F = \begin{pmatrix} F_1^0 \\ \vdots \\ F_N^0 \\ F_1^1 \\ \vdots \\ F_N^1 \\ \vdots \\ F_1^M \\ \vdots \\ F_N^M \end{pmatrix} \in ((M+1)N, 1) \quad \text{and} \quad T_{amb} = \begin{pmatrix} T_1^0 \\ \vdots \\ T_N^0 \\ T_1^1 \\ \vdots \\ T_N^1 \\ \vdots \\ T_1^M \\ \vdots \\ T_N^M \end{pmatrix} \in ((M+1)N, 1) \quad (11)$$

where the superscript m represents the time step in F_n^m and T_n^m , while the subscript n represents the spatial step. A general expression of one equation in the system is

$$F_n^m = A_{n,n-1}^m T_{n-1}^m + A_{n,n}^m T_n^m + A_{n,n+1}^m T_{n+1}^m - B_n^m T_n^{m-1} - C_n^m = 0 \quad (12)$$

where

$$A_{n,n-1}^m = - \left(\frac{\rho_n^{m-1} c_{p,n}^{m-1} u_{z,n}}{\Delta z} + \frac{2}{\Delta z} k_n^{m-1} \frac{1}{2\Delta z} \right) \quad (13)$$

$$A_{n,n}^m = \rho_n^{m-1} c_{p,n}^{m-1} \frac{1}{\Delta t} + \rho_n^{m-1} c_{p,n}^{m-1} u_{z,n} \frac{1}{\Delta z} + \frac{2}{\Delta z} k_n^{m-1} \left(\frac{2}{2\Delta z} \right) \quad (14)$$

$$A_{n,n+1}^m = - \frac{2}{\Delta z} k_n^{m-1} \frac{1}{2\Delta z} \quad (15)$$

$$B_n^m = \rho_n^{m-1} c_{p,n}^{m-1} \frac{1}{\Delta t} - \frac{1}{A_{amb,n}} c_{p,jet} \rho_{jet} Q_{jet,n} \quad (16)$$

and

$$C_n^m = \frac{1}{A_{amb,n}} c_{p,jet} \rho_{jet} Q_{jet,n} T_{jet} \quad (17)$$

Considering the initial condition, we have

$$F_n^0 = T_n^0 = T_{initial} \quad (18)$$

For boundary meshes, we used the Neumann boundary condition and assumed the temperature of the ghost boundary point, $T_0^m = T_1^m$, for the inlet mesh. Eq. (10) therefore becomes

$$\rho_1^{m-1} c_{p,1}^{m-1} \frac{T_1^m - T_1^{m-1}}{\Delta t} - \frac{2}{\Delta z} k_1^{m-1} \left(\frac{T_2^m - T_1^m}{2\Delta z} \right) = \frac{1}{A_{amb,1}} c_{p,jet} \rho_{jet} Q_{jet,1} (T_{jet} - T_1^{m-1}) \quad (19)$$

at the inlet mesh, and

$$F_1^m = A_{1,1,1}^m T_1^m + A_{1,1,2}^m T_2^m - B_1^m T_1^{m-1} - C_1^m = 0 \quad (20)$$

where

$$A_{1,1,1}^m = \rho_1^{m-1} c_{p,1}^{m-1} \frac{1}{\Delta t} + \frac{2}{\Delta z} k_1^{m-1} \left(\frac{2}{2\Delta z} \right) \quad (21)$$

$$A_{1,1,2}^m = - \frac{2}{\Delta z} k_1^{m-1} \frac{1}{2\Delta z} \quad (22)$$

$$B_1^m = \rho_1^{m-1} c_{p,1}^{m-1} \frac{1}{\Delta t} - \frac{1}{A_{amb,1}} c_{p,jet} \rho_{jet} Q_{jet,1} \quad (23)$$

and

$$C_1^m = \frac{1}{A_{amb,1}} c_{p,jet} \rho_{jet} Q_{jet,1} T_{jet} \quad (24)$$

Similar to the inlet mesh, we used the Neumann boundary condition and assumed the temperature of the ghost boundary point, $T_{N+1}^m = T_N^m$, for the outlet mesh. Eq. (10) therefore becomes

$$\begin{aligned} & \rho_N^{m-1} c_{p,N}^{m-1} \frac{T_N^m - T_N^{m-1}}{\Delta t} + \rho_N^{m-1} c_{p,N}^{m-1} u_{z,N} \frac{T_N^m - T_N^{m-1}}{\Delta z} + \frac{2}{\Delta z} k_N^{m-1} \left(\frac{T_N^m - T_{N-1}^m}{2\Delta z} \right) \\ & = \frac{1}{A_{amb,N}} c_{p,jet} \rho_{jet} Q_{jet,N} (T_{jet} - T_N^{m-1}) \end{aligned} \quad (25)$$

at the outlet mesh, and

$$F_N^m = A_{N,N-1}^m T_{N-1}^m + A_{N,N}^m T_N^m - B_N^m T_N^{m-1} - C_N^m = 0 \quad (26)$$

where

$$A_{N,N-1}^m = - \left(\frac{\rho_N^{m-1} c_{p,N}^{m-1} u_{z,N}}{\Delta z} + \frac{2}{\Delta z} k_N^{m-1} \frac{1}{2\Delta z} \right) \quad (27)$$

$$A_{N,N}^m = \rho_N^{m-1} c_{p,N}^{m-1} \frac{1}{\Delta t} + \rho_N^{m-1} c_{p,N}^{m-1} u_{z,N} \frac{1}{\Delta z} + \frac{2}{\Delta z} k_N^{m-1} \left(\frac{2}{2\Delta z} \right) \quad (28)$$

$$B_N^m = \rho_N^{m-1} c_{p,N}^{m-1} \frac{1}{\Delta t} - \frac{1}{A_{amb,N}} c_{p,jet} \rho_{jet} \dot{Q}_{jet,N} \quad (29)$$

and

$$C_N^m = \frac{1}{A_{amb,N}} c_{p,jet} \rho_{jet} \dot{Q}_{jet,N} T_{jet} \quad (30)$$

According to the discussions above, the 1-D thermal stratification model is a nonlinear system, because the parameters required for solving the temperature profile of the ambient fluid, including ρ_{amb} , $C_{p,amb}$, and k_{amb} , are themselves dependent on the temperature of the ambient fluid. The solution of the ambient fluid temperature profile, T_{amb} , at all time steps is therefore needed prior to conducting the adjoint sensitivity analysis (Cacuci and Ionescu-Bujor, 2000). Based on the temperature predictions, the mass density (ρ_{amb}), the heat capacity ($C_{p,amb}$), and the static thermal conductivity ($k_{c,amb}$) of the ambient fluid could be calculated according to sodium thermal properties:

$$\rho_{amb} = \begin{pmatrix} \rho(T_1^0) \\ \vdots \\ \rho(T_N^0) \\ \rho(T_1^1) \\ \vdots \\ \rho(T_N^1) \\ \vdots \\ \vdots \\ \rho(T_1^M) \\ \vdots \\ \rho(T_N^M) \end{pmatrix}_{\in((M+1)N,1)}, \quad C_{p,amb} = \begin{pmatrix} C_p(T_1^0) \\ \vdots \\ C_p(T_N^0) \\ C_p(T_1^1) \\ \vdots \\ C_p(T_N^1) \\ \vdots \\ \vdots \\ C_p(T_1^M) \\ \vdots \\ C_p(T_N^M) \end{pmatrix}_{\in((M+1)N,1)} \quad (31)$$

and

$$k_{c,amb} = \begin{pmatrix} k(T_1^0) \\ \vdots \\ k(T_N^0) \\ k(T_1^1) \\ \vdots \\ k(T_N^1) \\ \vdots \\ \vdots \\ k(T_1^M) \\ \vdots \\ k(T_N^M) \end{pmatrix}_{\in((M+1)N,1)} \quad (32)$$

It is pointed out that the heat transfer of the ambient fluid is enhanced by the turbulence caused by the impinging jet, and the effective thermal conductivity of the ambient fluid is higher than the static one. The relation between these two values will be further discussed in Section 3.2 with specific experimental conditions considered.

3.2. Experimental configuration and conditions

The experiment considered in the current study was performed in the Thermal Stratification Experimental Facility (TSTF), which was built at the University of Wisconsin-Madison (Schneider et al., 2018). The test section of the TSTF consisted of a cylindrical sodium tank with a diameter of about 30 cm and a height of about 130 cm. The inlet of the impinging jet was located at the bottom of the sodium tank, while the outlet of the sodium was located about 83 cm higher than the inlet, as shown in Fig. 1. An Upper Instrumentation Structure (UIS) that blocks the inlet of the impinging jets, the bottom of which was about $Z_{UIS} = 5\text{cm}$ from the jet inlet, was installed in the tank to emulate the in-vessel components located in the upper plenum of an SFR.

The experiment considered consisted of a 200 °C sodium jet, with a volumetric flow rate of $Q_{jet} = 0.38\text{L/s}$, impinging into the tank that was initially filled with 250 °C sodium. In this experiment, the impinging jet hit the bottom of the UIS after entering the sodium tank, and was not able to rise above it without dispersing in the ambient fluid. Because of the dispersion of the cooler jet, the temperature of the ambient fluid started to decrease since the beginning of the experiment, and finally converged to 200 °C at around 300 s elapsed time. We adopted a time step of 1 s and calculated the temperature of the ambient fluid for the first 300 s of the experiment in this study to ensure that the whole transient was covered. The total number of time steps was therefore $M = 300$. We only focused on the ambient fluid temperature below the outlet and used a total number of spatial steps $N = 83$, which made the spatial step about 1 cm.

The discretized form of the linear volumetric dispersion rate of the impinging jet in Eq. (9), Q_{jet} , was a vector of N entries, because it was independent of time in this study. By assuming a uniform dispersion rate, we have

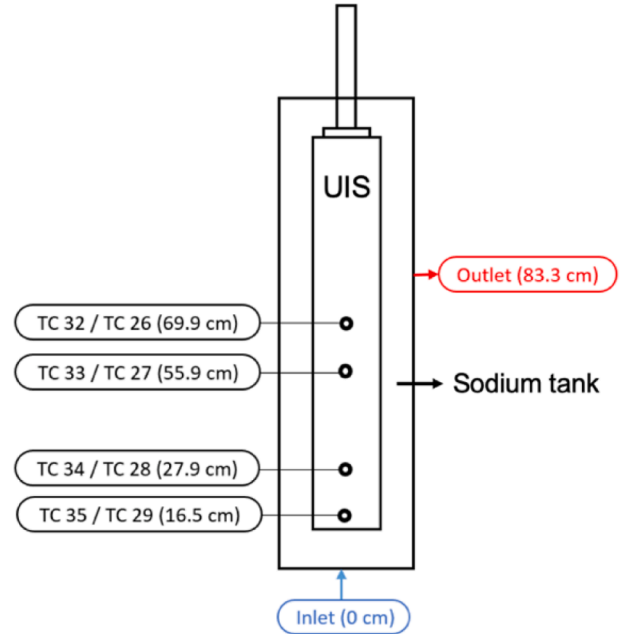


Fig. 1. The test section of the TSTF with positions of inlet and outlet (Lu et al., 2020).

$$Q_{jet}^* = Q_{jet} / Z_{UIS} \cdot \begin{pmatrix} 1 \\ 1 \\ 1 \\ 1 \\ 1 \\ 0 \\ \vdots \\ \vdots \\ \vdots \\ 0 \end{pmatrix} \in (N,1) \quad (33)$$

because the impinging jet was not able to rise above the bottom of the UIS.

Our research group recently developed a correlation between the effective and the static thermal conductivity of the ambient fluid (Lu et al., 2020) by using the inverse uncertainty quantification process, which is one of the data-assimilation methodologies. The newly-developed correlation was validated through both the experimental data acquired in the TSTF (Lu et al., 2020), which used sodium as the working fluid, as well as the experimental data acquired in the Gallium Thermal-hydraulic Experiment (GaTE) facility (Lu et al., 2020), which used gallium as the working fluid (Ward et al., 2019). According to the newly-developed correlation, the thermal conductivity of the ambient fluid, within the reach of the impinging jet, would be enhanced by the turbulence and became about 13.3 times higher for the experiment considered. The matrix of the effective thermal conductivity of the ambient fluid was therefore constructed as

$$k_{amb} = \begin{pmatrix} k_1^0 \\ \vdots \\ k_N^0 \\ k_1^1 \\ \vdots \\ k_N^1 \\ \vdots \\ k_1^M \\ \vdots \\ k_N^M \end{pmatrix} \in ((M+1)N,1) \quad (34)$$

where

$$k_n^m = 13.3k(T_n^m), \text{ when } m \neq 0 \text{ and } 1 \leq n \leq 5 \quad (35)$$

and

$$k_n^m = k(T_n^m), \text{ for other cases.} \quad (36)$$

3.3. Application of the discrete adjoint sensitivity method

We considered the temperature gradient of the ambient fluid as the figure of merit that best characterizes the thermal stratification phenomenon in this study. The vector variable of interest,

$$J = \begin{pmatrix} J_1^0 \\ \vdots \\ J_N^0 \\ J_1^1 \\ \vdots \\ J_N^1 \\ \vdots \\ J_1^M \\ \vdots \\ J_N^M \end{pmatrix} \in ((M+1)N,1) \quad (37)$$

was therefore defined as the temperature gradient of the ambient fluid with both space and time dependency. The elements of the vector, J_n^m , were approximated as

$$J_1^m = (T_2^m - T_1^m) / \Delta z \text{ at the inlet mesh,} \quad (38)$$

$$J_N^m = (T_N^m - T_{N-1}^m) / \Delta z \text{ at the outlet mesh,} \quad (39)$$

and

$$J_n^m = (T_{n+1}^m - T_{n-1}^m) / 2\Delta z \text{ else where} \quad (40)$$

by using the center difference approximation with a second-order spatial precision. The focus of this study was to investigate the sensitivities of the temperature gradient to four different parameters, Q_{jet} , T_{jet} , $C_{p,amb}$, and $k_{c,amb}$, which can be expressed in the form of matrices as

$$\delta J(T)_{\in((M+1)N,1)} = S_{\in((M+1)N,4)} \cdot \delta \theta_{\in(4,1)} \quad (41)$$

where

$$\theta = \begin{pmatrix} Q_{jet} \\ T_{jet} \\ C_{p,amb} \\ k_{c,amb} \end{pmatrix} \in (4,1) \quad (42)$$

The matrix S in Eq. (41) is the matrix of absolute sensitivity coefficients, which has the form of

$$S = \begin{pmatrix} S^0 \\ S^1 \\ \vdots \\ S^M \end{pmatrix} \in ((M+1)N,4) \quad (43)$$

where

$$S^m = \begin{pmatrix} S_{1,Q}^m & S_{1,T}^m & S_{1,C_p}^m & S_{1,k_c}^m \\ \vdots & \vdots & \vdots & \vdots \\ S_{N,Q}^m & S_{N,T}^m & S_{N,C_p}^m & S_{N,k_c}^m \end{pmatrix} \in (N,4) \quad (44)$$

According to Eq. (7), S will later be calculated as

$$S_{\in((M+1)N,4)} = \Phi_{\in((M+1)N,(M+1)N)}^T \cdot \frac{\partial F(T, \theta)}{\partial \theta} \in ((M+1)N,4) \quad (45)$$

where Φ is known as the adjoint vector, which is essentially the transpose matrix of the Lagrangian multipliers as indicated in Eq. (5). For better illustration of the computation of the sensitivity matrix S by using the discrete adjoint sensitivity method (which essentially involves some matrix manipulations), we separated the computation into three parts. Each part focused on the calculation of one necessary ingredient to eventually construct the large-size sensitivity matrix.

3.3.1. Computation of the adjoint solution Φ

The adjoint vectors Φ can be calculated from Eq. (6), which implies

$$\left(\frac{\partial F(\mathbf{T}, \theta)}{\partial \mathbf{T}}\right)^T_{\in((M+1)N, (M+1)N)} \cdot \Phi_{\in((M+1)N, (M+1)N)} = -\left(\frac{dJ(\mathbf{T})}{d\mathbf{T}}\right)^T_{\in((M+1)N, (M+1)N)} \quad (46)$$

By recalling the expression of F described in Eqs. (11)–(30), the Jacobian matrix $\frac{\partial F(\mathbf{T}, \theta)}{\partial \mathbf{T}}$ can be written in a matrix form as

$$\frac{\partial F(\mathbf{T}, \theta)}{\partial \mathbf{T}} = \begin{pmatrix} \frac{\partial F_1^0}{\partial T_1^0} & \dots & \frac{\partial F_1^0}{\partial T_N^0} & \frac{\partial F_1^0}{\partial T_1^1} & \dots & \frac{\partial F_1^0}{\partial T_N^1} & \dots & \dots & \dots & \frac{\partial F_1^0}{\partial T_1^M} & \dots & \frac{\partial F_1^0}{\partial T_N^M} \\ \vdots & \vdots \\ \frac{\partial F_N^0}{\partial T_1^0} & \dots & \frac{\partial F_N^0}{\partial T_N^0} & \frac{\partial F_N^0}{\partial T_1^1} & \dots & \frac{\partial F_N^0}{\partial T_N^1} & \dots & \dots & \dots & \frac{\partial F_N^0}{\partial T_1^M} & \dots & \frac{\partial F_N^0}{\partial T_N^M} \\ \frac{\partial F_1^1}{\partial T_1^0} & \dots & \frac{\partial F_1^1}{\partial T_N^0} & \frac{\partial F_1^1}{\partial T_1^1} & \dots & \frac{\partial F_1^1}{\partial T_N^1} & \dots & \dots & \dots & \frac{\partial F_1^1}{\partial T_1^M} & \dots & \frac{\partial F_1^1}{\partial T_N^M} \\ \vdots & \vdots \\ \frac{\partial F_N^1}{\partial T_1^0} & \dots & \frac{\partial F_N^1}{\partial T_N^0} & \frac{\partial F_N^1}{\partial T_1^1} & \dots & \frac{\partial F_N^1}{\partial T_N^1} & \dots & \dots & \dots & \frac{\partial F_N^1}{\partial T_1^M} & \dots & \frac{\partial F_N^1}{\partial T_N^M} \\ \vdots & \vdots \\ \vdots & \vdots \\ \frac{\partial F_1^M}{\partial T_1^0} & \dots & \frac{\partial F_1^M}{\partial T_N^0} & \frac{\partial F_1^M}{\partial T_1^1} & \dots & \frac{\partial F_1^M}{\partial T_N^1} & \dots & \dots & \dots & \frac{\partial F_1^M}{\partial T_1^M} & \dots & \frac{\partial F_1^M}{\partial T_N^M} \\ \vdots & \vdots \\ \frac{\partial F_N^M}{\partial T_1^0} & \dots & \frac{\partial F_N^M}{\partial T_N^0} & \frac{\partial F_N^M}{\partial T_1^1} & \dots & \frac{\partial F_N^M}{\partial T_N^1} & \dots & \dots & \dots & \frac{\partial F_N^M}{\partial T_1^M} & \dots & \frac{\partial F_N^M}{\partial T_N^M} \end{pmatrix}_{\in((M+1)N, (M+1)N)} \quad (47)$$

which can be further simplified to (the reason for this simplification will become apparent soon):

$$\frac{\partial F(\mathbf{T}, \theta)}{\partial \mathbf{T}} = \begin{pmatrix} \mathbf{A}^0 & \mathbf{0} & \dots & \dots & \dots & \dots & \mathbf{0} \\ \mathbf{B}^1 & \mathbf{A}^1 & \mathbf{0} & \dots & \dots & \dots & \mathbf{0} \\ \mathbf{0} & \mathbf{B}^2 & \mathbf{A}^2 & \mathbf{0} & \dots & \dots & \mathbf{0} \\ \vdots & \vdots & \vdots & \vdots & \vdots & \vdots & \vdots \\ \mathbf{0} & \dots & \dots & \mathbf{0} & \mathbf{B}^{M-1} & \mathbf{A}^{M-1} & \mathbf{0} \\ \mathbf{0} & \dots & \dots & \dots & \mathbf{0} & \mathbf{B}^M & \mathbf{A}^M \end{pmatrix}_{\in((M+1)N, (M+1)N)} \quad (48)$$

where

$$\mathbf{B}^m = - \begin{pmatrix} \mathbf{B}_1^m & \mathbf{0} & \dots & \dots & \mathbf{0} \\ \mathbf{0} & \mathbf{B}_2^m & \mathbf{0} & \dots & \mathbf{0} \\ \vdots & \vdots & & & \\ \mathbf{0} & \dots & \mathbf{0} & \mathbf{B}_{N-1}^m & \mathbf{0} \\ \mathbf{0} & \dots & \dots & \mathbf{0} & \mathbf{B}_N^m \end{pmatrix}_{\in(N, N)} \quad (49)$$

and

$$\mathbf{A}^m = \begin{pmatrix} \mathbf{A}_{1,1}^m & \mathbf{A}_{1,2}^m & \mathbf{0} & \dots & \dots & \dots & \mathbf{0} \\ \mathbf{A}_{2,1}^m & \mathbf{A}_{2,2}^m & \mathbf{A}_{2,3}^m & \mathbf{0} & \dots & \dots & \mathbf{0} \\ \mathbf{0} & \mathbf{A}_{3,1}^m & \mathbf{A}_{3,2}^m & \mathbf{A}_{3,3}^m & \mathbf{0} & \dots & \mathbf{0} \\ \vdots & \vdots & \vdots & \vdots & \vdots & \vdots & \vdots \\ \mathbf{0} & \dots & \mathbf{0} & \mathbf{A}_{N-2, N-3}^m & \mathbf{A}_{N-2, N-2}^m & \mathbf{A}_{N-2, N-1}^m & \mathbf{0} \\ \mathbf{0} & \dots & \dots & \mathbf{0} & \mathbf{A}_{N-1, N-2}^m & \mathbf{A}_{N-1, N-1}^m & \mathbf{A}_{N, N-1}^m \\ \mathbf{0} & \dots & \dots & \dots & \mathbf{0} & \mathbf{A}_{N, N-1}^m & \mathbf{A}_{N, N}^m \end{pmatrix}_{\in(N, N)} \quad (50)$$

when $m \neq 0$. $A^0 = I_{\in(N,N)}$, and the expressions of B_i^m and A_{ij}^m are given in Section 3.1.

By calling the expression of J described in Eqs. (37)–(40), $\frac{dJ(T)}{dT}$ can be written in a matrix form as

inversion of a matrix with more than 620 million entries, which surpasses the capability of a common personal computer. In this case, we had to solve for the submatrices of Φ by expressing it as

$$\Phi = (\Phi^0 \quad \Phi^1 \quad \dots \quad \Phi^M)_{\in((M+1)N, (M+1)N)} \quad (54)$$

$$\frac{dJ(T)}{dT} = \begin{pmatrix} \frac{\partial J_1^0}{\partial T_1^0} & \dots & \frac{\partial J_N^0}{\partial T_N^0} & \frac{\partial J_1^0}{\partial T_1^1} & \dots & \frac{\partial J_N^0}{\partial T_N^1} & \dots & \dots & \dots & \frac{\partial J_1^0}{\partial T_1^M} & \dots & \frac{\partial J_N^0}{\partial T_N^M} \\ \vdots & \vdots \\ \frac{\partial J_N^0}{\partial T_1^0} & \dots & \frac{\partial J_N^0}{\partial T_N^0} & \frac{\partial J_N^0}{\partial T_1^1} & \dots & \frac{\partial J_N^0}{\partial T_N^1} & \dots & \dots & \dots & \frac{\partial J_N^0}{\partial T_1^M} & \dots & \frac{\partial J_N^0}{\partial T_N^M} \\ \frac{\partial J_1^1}{\partial T_1^0} & \dots & \frac{\partial J_1^1}{\partial T_N^0} & \frac{\partial J_1^1}{\partial T_1^1} & \dots & \frac{\partial J_1^1}{\partial T_N^1} & \dots & \dots & \dots & \frac{\partial J_1^1}{\partial T_1^M} & \dots & \frac{\partial J_1^1}{\partial T_N^M} \\ \vdots & \vdots \\ \frac{\partial J_N^1}{\partial T_1^0} & \dots & \frac{\partial J_N^1}{\partial T_N^0} & \frac{\partial J_N^1}{\partial T_1^1} & \dots & \frac{\partial J_N^1}{\partial T_N^1} & \dots & \dots & \dots & \frac{\partial J_N^1}{\partial T_1^M} & \dots & \frac{\partial J_N^1}{\partial T_N^M} \\ \vdots & \vdots \\ \vdots & \vdots \\ \frac{\partial J_1^M}{\partial T_1^0} & \dots & \frac{\partial J_1^M}{\partial T_N^0} & \frac{\partial J_1^M}{\partial T_1^1} & \dots & \frac{\partial J_1^M}{\partial T_N^1} & \dots & \dots & \dots & \frac{\partial J_1^M}{\partial T_1^M} & \dots & \frac{\partial J_1^M}{\partial T_N^M} \\ \vdots & \vdots \\ \frac{\partial J_N^M}{\partial T_1^0} & \dots & \frac{\partial J_N^M}{\partial T_N^0} & \frac{\partial J_N^M}{\partial T_1^1} & \dots & \frac{\partial J_N^M}{\partial T_N^1} & \dots & \dots & \dots & \frac{\partial J_N^M}{\partial T_1^M} & \dots & \frac{\partial J_N^M}{\partial T_N^M} \end{pmatrix}_{\in((M+1)N, (M+1)N)} \quad (51)$$

which can be further simplified to

$$\frac{dJ(T)}{dT} = \begin{pmatrix} \mathbf{D} & \mathbf{0} & \dots & \dots & \mathbf{0} \\ \mathbf{0} & \mathbf{D} & \mathbf{0} & \dots & \mathbf{0} \\ \vdots & \vdots & \vdots & \vdots & \vdots \\ \mathbf{0} & \dots & \mathbf{0} & \mathbf{D} & \mathbf{0} \\ \mathbf{0} & \dots & \dots & \mathbf{0} & \mathbf{D} \end{pmatrix}_{\in((M+1)N, (M+1)N)} \quad (52)$$

where

$$\mathbf{D} = \frac{1}{\Delta z} \begin{pmatrix} -1 & 1 & 0 & \dots & \dots & \dots & 0 \\ -\frac{1}{2} & 0 & \frac{1}{2} & 0 & \dots & \dots & 0 \\ 0 & -\frac{1}{2} & 0 & \frac{1}{2} & 0 & \dots & 0 \\ \vdots & \vdots & \vdots & \vdots & \vdots & \vdots & \vdots \\ 0 & \dots & 0 & -\frac{1}{2} & 0 & \frac{1}{2} & 0 \\ 0 & \dots & \dots & 0 & -\frac{1}{2} & 0 & \frac{1}{2} \\ 0 & \dots & \dots & \dots & 0 & -1 & 1 \end{pmatrix}_{\in(N,N)} \quad (53)$$

Now that both $\frac{\partial F(T, \theta)}{\partial T}$ and $\frac{dJ(T)}{dT}$ have been computed, the adjoint vector Φ can be computed by directly inverting the Jacobian matrix $\frac{\partial F(T, \theta)}{\partial T}$. However, the computational expense of this operation increases quadratically with the dimension of the matrices. For example, in this study, we have $M = 300$ and $N = 83$. Directly solving for Φ requires the

where

$$\Phi^m = \begin{pmatrix} \Phi_0^m \\ \Phi_1^m \\ \vdots \\ \Phi_M^m \end{pmatrix}_{\in((M+1)N, N)} \quad (55)$$

The submatrices $\Phi_j^m \in (N, N)$ of Φ^m can then be solved by combining Eqs. (46)–(53):

$$\Phi_j^m = \begin{cases} \mathbf{0} & \text{when } j > m, \\ ((A^j)^T)^{-1} \mathbf{D} & \text{when } j = m, \\ -((A^j)^T)^{-1} (\mathbf{B}^{j+1} \Phi_{j+1}^m) & \text{when } 0 < j < m, \\ -(\mathbf{B}^{j+1} \Phi_{j+1}^m) & \text{when } j = 0, \end{cases} \quad (56)$$

which implies that the Φ^m matrices are independent of each other.

3.3.2. Computation of the Jacobian matrix $\frac{\partial F(T, \theta)}{\partial \theta}$

By recalling the expression of F described in Eqs. (11)–(30) and the expression of θ described in Eq. (42), $\frac{\partial F(T, \theta)}{\partial \theta}$ can be written in matrix form as

$$\frac{\partial \mathbf{F}(\mathbf{T}, \boldsymbol{\theta})}{\partial \boldsymbol{\theta}} = \begin{pmatrix} 0 & 0 & 0 & 0 \\ \vdots & \vdots & \vdots & \vdots \\ 0 & 0 & 0 & 0 \\ \frac{\partial F_1^1}{\partial Q_{jet}} & \frac{\partial F_1^1}{\partial T_{jet}} & \frac{\partial F_1^1}{\partial C_{p,amb}} & \frac{\partial F_1^1}{\partial k_{c,amb}} \\ \vdots & \vdots & \vdots & \vdots \\ \frac{\partial F_N^1}{\partial Q_{jet}} & \frac{\partial F_N^1}{\partial T_{jet}} & \frac{\partial F_N^1}{\partial C_{p,amb}} & \frac{\partial F_N^1}{\partial k_{c,amb}} \\ \vdots & \vdots & \vdots & \vdots \\ \vdots & \vdots & \vdots & \vdots \\ \vdots & \vdots & \vdots & \vdots \\ \frac{\partial F_1^M}{\partial Q_{jet}} & \frac{\partial F_1^M}{\partial T_{jet}} & \frac{\partial F_1^M}{\partial C_{p,amb}} & \frac{\partial F_1^M}{\partial k_{c,amb}} \\ \vdots & \vdots & \vdots & \vdots \\ \frac{\partial F_N^M}{\partial Q_{jet}} & \frac{\partial F_N^M}{\partial T_{jet}} & \frac{\partial F_N^M}{\partial C_{p,amb}} & \frac{\partial F_N^M}{\partial k_{c,amb}} \end{pmatrix} \in ((M+1)N, 4) \quad (57)$$

where

$$\frac{\partial F_n^m}{\partial Q_{jet}} = \frac{1}{A_{amb,n}} C_{p,jet} \rho_{jet} (T_n^{m-1} - T_{jet}) \frac{Q_{jet}'(n)}{Q_{jet}} \quad (58)$$

$$\frac{\partial F_n^m}{\partial T_{jet}} = -\frac{1}{A_{amb,n}} C_{p,jet} \rho_{jet} Q_{jet}'(n), \quad (59)$$

$$\frac{\partial F_n^m}{\partial C_{p,amb}} = \begin{cases} \frac{1}{\Delta t} \rho_n^{m-1} (T_n^m - T_n^{m-1}) & \text{when } n = 1, \\ \frac{u_{\varepsilon,n}}{\Delta Z} \rho_n^{m-1} (T_n^m - T_{n-1}^m) + \frac{1}{\Delta t} \rho_n^{m-1} (T_n^m - T_n^{m-1}) & \text{when } 1 < n \leq N. \end{cases} \quad (60)$$

$$\frac{\partial F_n^m}{\partial k_{c,amb}} = \begin{cases} \frac{13.3}{\Delta z^2} (T_1^m - T_2^m) & \text{when } n = 1, \\ \frac{13.3}{\Delta z^2} (-T_{m-1}^m + 2T_m^m - T_{m+1}^m) & \text{when } 1 < n \leq 5, \\ \frac{1}{\Delta z^2} (-T_{m-1}^m + 2T_m^m - T_{m+1}^m) & \text{when } 5 < n < N, \\ \frac{1}{\Delta z^2} (T_N^m - T_{N-1}^m) & \text{when } n = N. \end{cases} \quad (61)$$

3.3.3. Computation of the sensitivity matrix S

Now that both Φ and $\frac{\partial \mathbf{F}(\mathbf{T}, \boldsymbol{\theta})}{\partial \boldsymbol{\theta}}$ have been computed, S can be calculated according to Eq. (45) as

$$\begin{pmatrix} S^0 \\ S^1 \\ \vdots \\ S^M \end{pmatrix} \in ((M+1)N, 4) = \begin{pmatrix} (\Phi^0)^T \\ (\Phi^1)^T \\ \vdots \\ (\Phi^M)^T \end{pmatrix} \in ((M+1)N, (M+1)N) \cdot \frac{\partial \mathbf{F}(\mathbf{T}, \boldsymbol{\theta})}{\partial \boldsymbol{\theta}} \in ((M+1)N, 4) \quad (62)$$

When the absolute sensitivity is desired at a specific time step m, it can be calculated as

$$S_{\in(N,4)}^m = \begin{pmatrix} S_{1,Q}^m & S_{1,T}^m & S_{1,C_p}^m & S_{1,k_c}^m \\ \vdots & \vdots & \vdots & \vdots \\ S_{N,Q}^m & S_{N,T}^m & S_{N,C_p}^m & S_{N,k_c}^m \end{pmatrix} \in (N, 4) \\ = (\Phi^m)^T \in (N, (M+1)N) \cdot \frac{\partial \mathbf{F}(\mathbf{T}, \boldsymbol{\theta})}{\partial \boldsymbol{\theta}} \in ((M+1)N, 4) \quad (63)$$

without the computation of the rest of Φ . The relative sensitivity,

$$S_r = \begin{pmatrix} S_r^0 \\ S_r^1 \\ \vdots \\ S_r^M \end{pmatrix} \in ((M+1)N, 4) \quad (64)$$

can then be further computed as

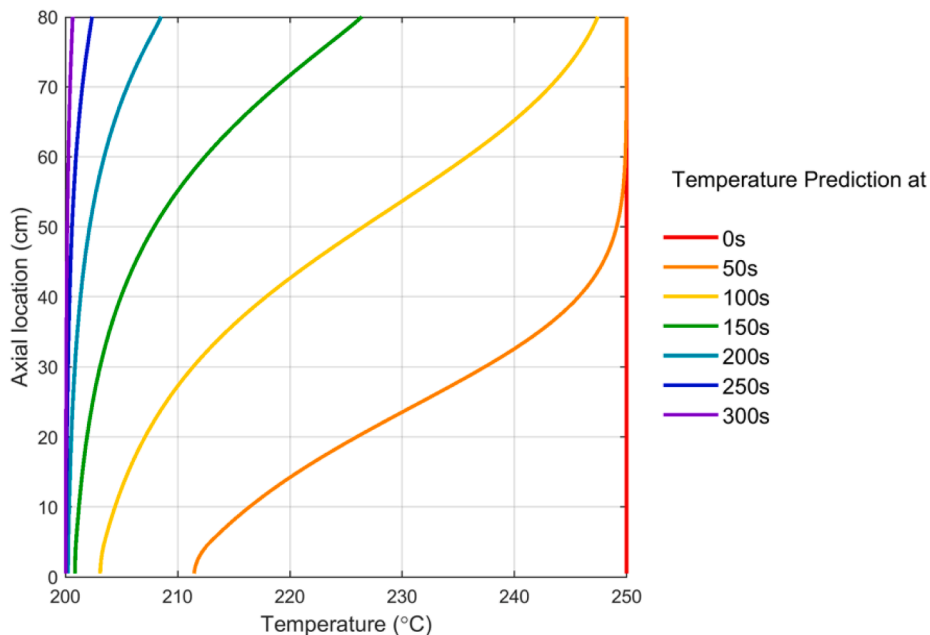


Fig. 2. Temperature prediction for the experiment at different elapsed times.

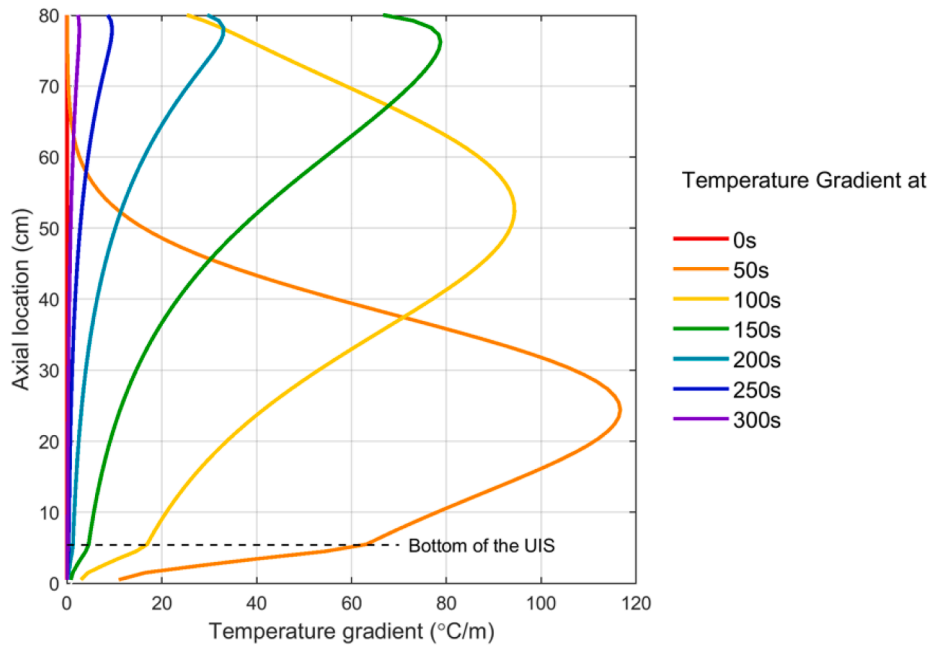


Fig. 3. Temperature gradient for the experiment at different elapsed times.

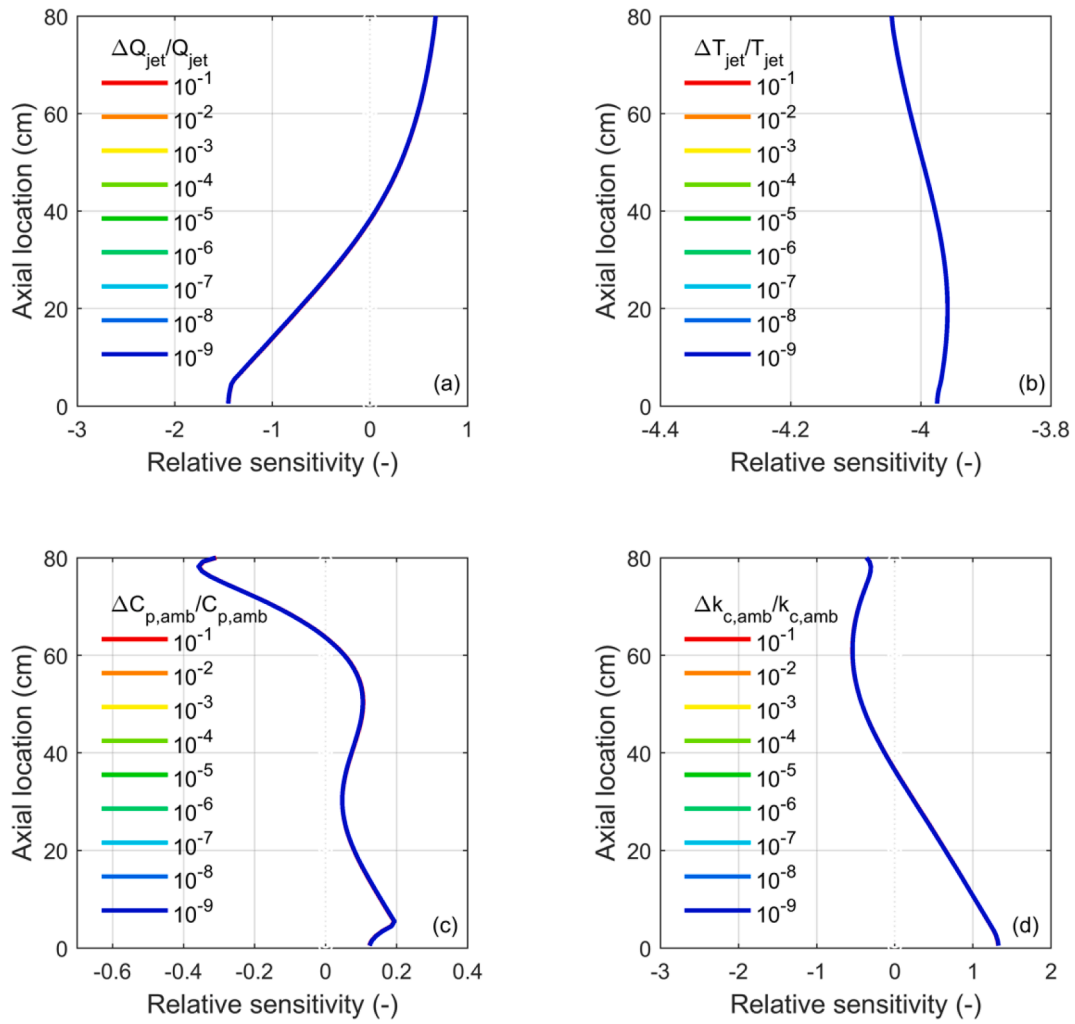


Fig. 4. Relative sensitivities of temperature gradient to the four parameters with different $\Delta\theta/\theta$.

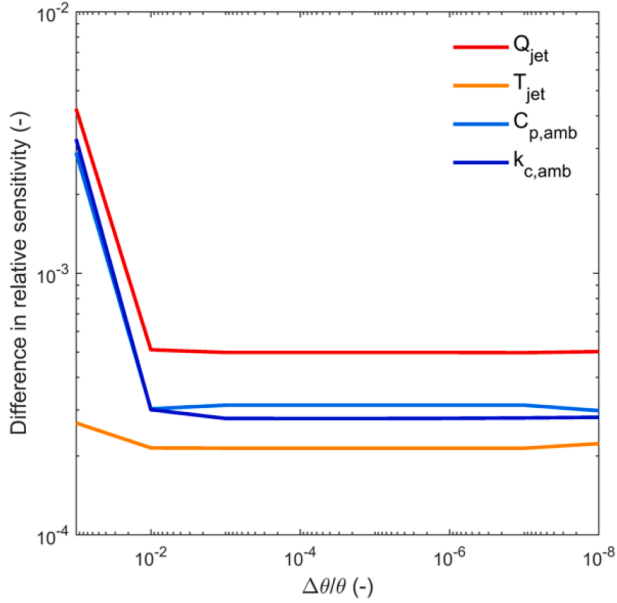


Fig. 5. Maximum absolute differences in relative sensitivities, caused by the use of different $\Delta\theta/\theta$.

Table 1
Maximum absolute differences in relative sensitivities calculated by both methods.

Parameter investigated	Max. abs. difference in relative sensitivities	Axial location of occurrence (cm)	Forward method	Adjoint method
Q_{jet}	0.02	1.5	-1.45	-1.47
T_{jet}	0.04	20.4	-3.96	-4.00
$C_{p,amb}$	0.01	1.5	0.13	0.14
$k_{c,amb}$	0.03	0.5	1.33	1.36

large adjoint matrix, followed by efficient matrix manipulations. The matrix construction and multiplication are relatively straightforward and easy to implement. The computational cost, however, may become prohibitive if one intends to produce the large matrix via the direct matrix inversion techniques. Fortunately, the adjoint matrix normally appears to be sparse due to the nature of the physics model. Thus, algebraic matrix arrangement techniques, such as the one presented in Section 3.3.2, can be identified and greatly simplify the matrix manipulation procedure. Another noteworthy disadvantage of the discrete adjoint method would be the invasive property of the method, which means one must know the computational schemes of the forward model before a successful implementation of discrete adjoint method. This disadvantage may limit its application to the current product-level software, whose source code is not transparent to end users.

$$S_r^m \in (N, 4) = \begin{pmatrix} S_{1,Q}^m \cdot \frac{Q_{jet}}{J_1^m} & S_{1,T}^m \cdot \frac{T_{jet}}{J_1^m} & S_{1,C_p}^m \cdot \frac{C_p(T_N^m)}{J_1^m} & S_{1,k_c}^m \cdot \frac{k(T_N^m)}{J_1^m} \\ \vdots & \vdots & \vdots & \vdots \\ S_{N,Q}^m \cdot \frac{Q_{jet}}{J_N^m} & S_{N,T}^m \cdot \frac{T_{jet}}{J_N^m} & S_{N,C_p}^m \cdot \frac{C_p(T_N^m)}{J_N^m} & S_{N,k_c}^m \cdot \frac{k(T_N^m)}{J_N^m} \end{pmatrix} \in (N,4) \quad (65)$$

With the application of the discrete adjoint sensitivity method outlined above, some general remarks on the pros and cons of this method can be made. The discrete adjoint method basically takes the advantages of the linearization process of the governing equation, which makes the method applicable to time-dependent and nonlinear problems. In this regard, the discrete adjoint method is apparently a very powerful sensitivity analysis approach that is extendable to multiple responses with multiple input parameters. This feature is best demonstrated by Eq. (54), in which all the adjoints to various responses are encapsulated in a

4. Results of the discrete adjoint sensitivity calculations

4.1. Verification of the discrete adjoint sensitivity method

The ambient fluid temperature profile during the experiment, described in Section 3.2, was calculated by solving the nonlinear system F described in Eqs. (11)–(30). The temperature predictions at different elapsed times are plotted in Fig. 2.

During the experiment, the ambient fluid in the sodium tank initially had a uniform temperature profile of 250 °C. Due to the dispersion of the impinging sodium at 200 °C, the ambient fluid around the bottom of the tank started to cool down first. The temperature of the ambient fluid at higher locations then started to decrease through heat transfer, and a large temperature gradient was developed. The temperature of the ambient fluid in the whole tank finally converged to 200 °C at around 300 s elapsed time. The temperature gradient, considered as the figure of merit in this study, was calculated and plotted in Fig. 3.

Discontinuities in temperature gradient curves were observed at the

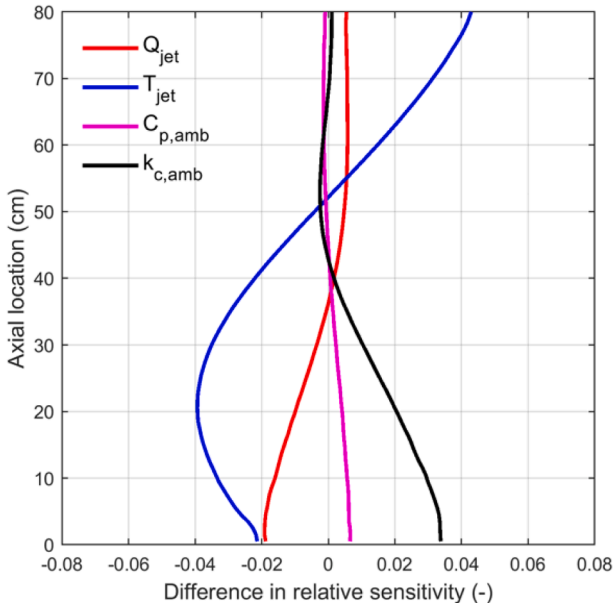


Fig. 6. Differences in the relative sensitivities calculated by both methods.

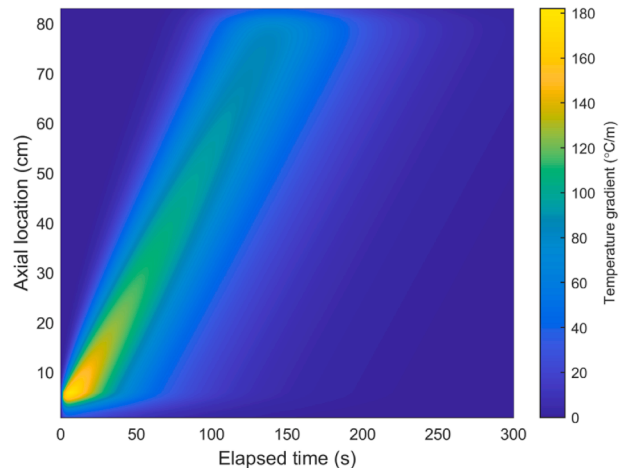


Fig. 7. Temperature gradient map throughout the experimental transient.

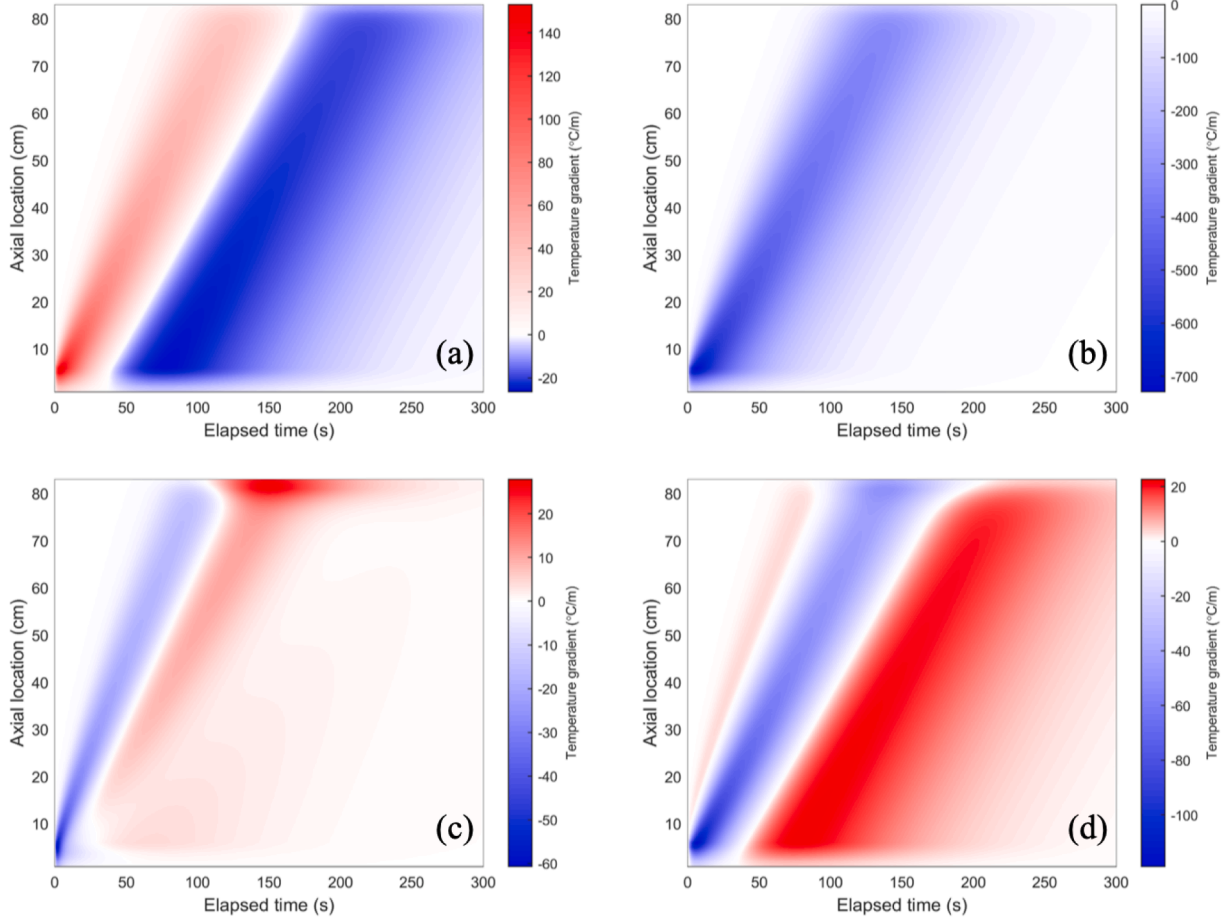


Fig. 8. Semi-relative sensitivity map of temperature gradient to (a) Q_{jet} , (b) T_{jet} , (c) $C_{p,amb}$, and (d) $k_{c,amb}$, at different axial locations throughout the experiment.

Table 2

Semi-relative sensitivities of the temperature gradient to the four parameters at 50 s, 150 s, and 250 s elapsed time of the experiment.

Axial location (cm)	50 s elapsed time				150 s elapsed time				250 s elapsed time			
	Q_{jet}	T_{jet}	$C_{p,amb}$	$k_{c,amb}$	Q_{jet}	T_{jet}	$C_{p,amb}$	$k_{c,amb}$	Q_{jet}	T_{jet}	$C_{p,amb}$	$k_{c,amb}$
70	0.33	-1.56	-0.99	0.66	4.82	-280.58	7.65	-12.27	-12.89	-26.58	0.59	12.45
50	15.63	-80.02	-16.23	0.70	-20.22	-138.85	1.40	19.23	-7.40	-10.35	0.64	6.83
30	62.86	-440.28	1.51	-64.10	-20.16	-55.16	1.91	18.53	-3.81	-4.02	0.42	3.42
10	-4.66	-296.69	2.78	2.44	-12.78	-21.41	1.64	11.27	-1.85	-1.57	0.23	1.63

bottom of the UIS, where the impinging jet was blocked. Because of the nearly uniform temperature profile at both the beginning and the end of the transient, the corresponding temperature gradient profiles were about zero. Compared to other elapsed times, the temperature profile had the largest axial-location dependency at 100 s elapsed time, and had a large temperature gradient. Therefore, we performed the verification of the adjoint sensitivity method at this elapsed time by comparing its results to that obtained through the forward sensitivity method.

The forward sensitivity analysis procedure is relatively straightforward. Small perturbations were introduced to each of the four parameters shown in Eq. (42) around their nominal values, and the corresponding variations in temperature gradient of the ambient fluid were calculated. The absolute sensitivity of the ambient fluid temperature gradient to the parameter can then be estimated by using the center-finite-difference scheme:

$$S_{\theta} = \frac{J(T(\theta_0 + \Delta\theta)) - J(T(\theta_0 - \Delta\theta))}{2\Delta\theta} \quad (66)$$

where $\theta = Q_{jet}, T_{jet}, C_{p,amb},$ or $k_{c,amb}$, and θ_0 represents its nominal value.

Once the absolute sensitivity is obtained, it can be converted to the relative sensitivity by using Eq. (65). The S_{θ} calculated this way is dependent on the $\Delta\theta$ employed. We therefore performed a sensitivity analysis on $\Delta\theta$ for each of the four parameters to ensure the convergence of the S_{θ} .

The relative sensitivities of temperature gradient to the four parameters, calculated at 100 s elapsed time, by using different $\Delta\theta/\theta$, are compared in Fig. 4. The relative sensitivity of temperature gradient to Q_{jet} varied from around -1.5, at the bottom of the tank, to around 0.7, at the top of the tank. This suggested that an increase in Q_{jet} would decrease the temperature gradient at the bottom of the tank, but increase the temperature gradient at the top of the tank. The relative sensitivity of temperature gradient to T_{jet} stayed around -4, which suggested that an increase in T_{jet} would decrease the temperature gradient. The relative sensitivity of temperature gradient to $C_{p,amb}$ varied from around 0.2, at the bottom of the tank, to around -0.4, at the top of the tank. This suggested that an increase in $C_{p,amb}$ would increase the temperature gradient at the bottom of the tank, but decrease the temperature gradient at the top of the tank. The relative sensitivity of

temperature gradient to $k_{c,amb}$ varied from around 1.5, at the bottom of the tank, to around -0.5 , at the top of the tank. This suggested that an increase in $k_{c,amb}$ would increase the temperature gradient at the bottom of the tank, but decrease the temperature gradient at the top of the tank.

The maximum absolute differences in the relative sensitivities, caused by the use of different $\Delta\theta/\theta$, with respect to that calculated with $\Delta\theta/\theta = 10^{-9}$, are summarized in Fig. 5. For all of the four parameters, the use of a $\Delta\theta/\theta = 10^{-2}$ would cause a difference smaller than 10^{-3} , and was therefore considered small enough for an accurate calculation of the relative sensitivity of temperature gradient at 100 s elapsed time by using the forward sensitivity method. In this study, a common value of $\Delta\theta/\theta = 10^{-9}$ was employed in all forward sensitivity calculations for being conservative.

The relative sensitivities calculated were then used for the verification of the adjoint sensitivity method. The differences of the relative sensitivities calculated by both methods are plotted in Fig. 6 for each of the four parameters at different axial locations. The maximum absolute differences in the relative sensitivities were less than 0.02, 0.05, 0.01, and 0.03 for Q_{jet} , T_{jet} , $C_{p,amb}$, and $k_{c,amb}$, respectively. These values were more than one order of magnitude smaller than the relative sensitivities calculated by both methods at the same locations, as summarized in Table 1. These results confirmed the correctness and accuracy of the sensitivities calculated by both the forward and the adjoint sensitivity methods.

4.2. More results from the discrete adjoint sensitivity method

The temperature gradient map of the ambient fluid at different axial locations throughout the experimental transient was predicted by the 1-D model and pictorially illustrated in Fig. 7. As shown in Fig. 7, the peak value of the temperature gradient appeared around the bottom of the tank at the beginning of the experiment, and moved upward with an increasing elapsed time. The maximum of the temperature gradient was about $180\text{ }^\circ\text{C/m}$. It occurred at 7 s elapsed time and 5 cm away from the bottom of the tank, where the bottom of the UIS was located. The temperature gradient in the whole tank decreased to zero at around 300 s elapsed time, which justified the convergence of the temperature of the ambient fluid to that of the impinging jet.

The absolute sensitivities, in the sense of absolute changes in the temperature gradient caused by absolute changes in the parameters, cannot provide a direct comparison of the impact of different parameters on the temperature gradient. The relative sensitivities, in the sense of relative changes in the temperature gradient caused by relative changes in the parameters, may provide unphysical values when the temperature gradient is zero. Therefore, the so-called semi-relative sensitivities, in the sense of absolute changes in the temperature gradient caused by relative changes in the parameters, were employed in the following analysis. They are evaluated as

$$S_{sr}^m \in (N, 4) = \begin{pmatrix} S_{1,Q}^m \cdot Q_{jet} & S_{1,T}^m \cdot T_{jet} & S_{1,C_p}^m \cdot C_p(T_1^m) & S_{1,k_c}^m \cdot k(T_1^m) \\ \vdots & \vdots & \vdots & \vdots \\ S_{N,Q}^m \cdot Q_{jet} & S_{N,T}^m \cdot T_{jet} & S_{N,C_p}^m \cdot C_p(T_N^m) & S_{N,k_c}^m \cdot k(T_N^m) \end{pmatrix}_{\in(N,4)} \quad (67)$$

which avoided both issues mentioned above. The semi-relative sensitivities of temperature gradient to each of the four parameters, namely Q_{jet} , T_{jet} , $C_{p,amb}$ and $k_{c,amb}$, were generated by the one-time calculation of the discrete adjoint sensitivity method. The corresponding sensitivity maps are shown in Fig. 8 (a) - (d) respectively, and the semi-relative sensitivities of the temperature gradient to the four parameters at 50 s, 150 s, and 250 s elapsed time of the experiment are summarized respectively in Table 2 to show the overall behavior of these sensitivities.

By comparing Fig. 8 with Fig. 7, we can observe that the semi-relative sensitivities of the temperature gradient to the four

parameters peaked at the same locations as the temperature gradient. This implies that a change in these four parameters of investigation had a larger impact on the temperature gradient when the temperature gradient was larger. As indicated in Fig. 8 and Table 2, perturbations in Q_{jet} , $C_{p,amb}$, and $k_{c,amb}$ would introduce either positive or negative changes to the temperature gradient of the ambient fluid, depending on the axial location and the elapsed time of the experiment. An increase in Q_{jet} exacerbated the thermal stratification phenomenon, and therefore further increased the temperature gradient at its peak and decreased the temperature gradient around the peak, which made the peak more significant. An increase in $C_{p,amb}$ and $k_{c,amb}$, on the contrary, alleviated the thermal stratification phenomenon by decreasing the temperature gradient at its peak and increasing the temperature gradient around the peak, which flattened the curve of temperature gradient. Different from the other three parameters, an increase in T_{jet} always decreased the temperature gradient. This is because when T_{jet} increased, the difference between T_{jet} and the initial temperature of the ambient fluid decreased. The temperature gradient caused by the injection of the jet therefore also decreased. At 7 s elapsed time and 5 cm from the bottom of the tank, where the maximum of the temperature gradient occurred, the semi-relative sensitivity of the temperature gradient was about $150\text{ }^\circ\text{C/m}$ for Q_{jet} , $-730\text{ }^\circ\text{C/m}$ for T_{jet} , $-30\text{ }^\circ\text{C/m}$ for $C_{p,amb}$, and $-120\text{ }^\circ\text{C/m}$ for $k_{c,amb}$. This suggested that the impact of T_{jet} on the temperature gradient was several times higher than that of the other three parameters.

5. Summary and conclusions

In this work, we performed a parameter sensitivity analysis to the 1-D thermal stratification model, which was recently developed in our research group for the prediction of the coolant temperature profile in the hot plenum of SFRs during transients. The reference transient considered in the study was an experiment performed in the TSTF, which was built at the University of Wisconsin-Madison. The experiment consisted of a $200\text{ }^\circ\text{C}$ sodium jet, with a volumetric flow rate of $Q_{jet} = 0.38\text{ L/s}$, impinging into a cylindrical test section, initially filled with $250\text{ }^\circ\text{C}$ sodium.

We considered the temperature gradient of the ambient fluid in the test section as the figure of merit for the sensitivity analysis, because it serves as a good quantitative metric reflecting the severity of the thermal stratification phenomenon. We investigated the sensitivity of the temperature gradient with respect to four parameters, including two inlet parameters, namely the jet volumetric flow rate Q_{jet} and the jet temperature T_{jet} , and two thermal-hydraulic parameters, namely the heat capacity $C_{p,amb}$ and the static thermal conductivity $k_{c,amb}$ of the ambient fluid in the test section. The sensitivity analysis was performed through the use of both the conventional forward sensitivity method and the adjoint sensitivity method. In the forward sensitivity method, small perturbations were introduced to the parameters to ensure a good accuracy. In the adjoint sensitivity method, the discrete adjoint sensitivity analysis procedure was employed to take the advantages of the numerical discretization form of the adjoint equation. The difference in the sensitivity coefficients, obtained from both sensitivity methods, was negligible, which offered a cross verification of both sensitivity methods.

The sensitivity maps of the four parameters of interest were obtained by the discrete adjoint sensitivity method. Considering four parameters in the sensitivity analysis in this study, the calculations performed by using the discrete adjoint sensitivity method was about 50% cheaper than that performed by using the conventional forward sensitivity method. The sensitivities obtained suggested that depending on the axial location and the elapsed time of the experiment, perturbations in Q_{jet} , $C_{p,amb}$, and $k_{c,amb}$ could introduce either positive or negative changes to the temperature gradient of the ambient fluid. However, an increase in T_{jet} always decreased the temperature gradient. This was expected because when the temperature of the jet increased, its difference to the initial temperature of the ambient fluid decreased. The temperature

gradient caused by the injection of the jet therefore decreased. Moreover, the impact of T_{jet} on the maximum temperature gradient was found to be several times higher than that caused by the other three parameters. This observation indicated that additional attention needs to be paid to the occurrence of thermal stratification in the hot plenum of an SFR when the impinging jet has a large temperature change.

The detailed application procedure of the discrete adjoint sensitivity method to the 1-D thermal stratification model, outlined in this paper, also provided a step-by-step example of the use of the discrete adjoint sensitivity method on time-dependent nonlinear systems. This example is expected to flatten the learning curve of researchers who are new to this method. Regarding future perspective to the current work, we are interested in performing the sensitivity analysis by using the alternative continuous adjoint sensitivity analysis method as a demonstration of the method viability. The importance function associated with the response of interest, obtained through the continuous adjoint sensitivity analysis procedure, is expected to provide additional physical insights to the problem of investigation. We are also interested in exploring uncertainty propagation mechanisms within the system of interest by using the sensitivity information gained from the sensitivity analysis.

CRedit authorship contribution statement

Cihang Lu: Writing-original draft, Data curation, Formal analysis.
Zeyun Wu: Supervision, Writing - review & editing.

Declaration of Competing Interest

The authors declare that they have no known competing financial interests or personal relationships that could have appeared to influence the work reported in this paper.

References

- Cacuci, D.G., 1981. Sensitivity theory for nonlinear systems. II. Extensions to additional classes of responses. *J. Mathemat. Phys.* 22 (12), 2803–2812.
- Cacuci, D.G., 1981. Sensitivity theory for nonlinear systems. I. Nonlinear functional analysis approach. *J. Mathemat. Phys.* 22 (12), 2794–2802.
- Cacuci, D.G., Ionescu-Bujor, M., 2000. Adjoint sensitivity analysis of the RELAP5/MOD3.2 two-fluid thermal-hydraulic code system - I: theory. *Nucl. Sci. Eng.* 136, 59–84.
- Cacuci, D.G., Wacholder, E., 1982. Adjoint sensitivity analysis for transient two-phase flow. *Nucl. Sci. Eng.* 82, 461–468.
- Cacuci, D.G., Weber, C.F., Oblow, E.M., Marable, J.H., 1980. Sensitivity theory for general systems of nonlinear equations. *Nucl. Sci. Eng.* 75, 88–110.
- Cacuci, D.G., Fang, R., Ilic, M., Badea, M.C., 2016. A heat conduction and convection analytical benchmark for adjoint solution verification of computational fluid dynamics codes used in reactor design. *Nucl. Sci. Eng.* 182, 452–480.
- Cao, Y., Li, S., Petzold, L., Serban, R., 2003. Adjoint sensitivity analysis for differential-algebraic equations: the adjoint DAE system and its numerical solution. *SIAM J. Sci. Comput.* 24 (3), 1076–1089.
- Drzewiecki, T.J., 2013. Adjoint Based Uncertainty Quantification and Sensitivity Analysis for Nuclear Thermal-Fluid Codes. Ph.D. Dissertation. University of Michigan.
- A. C. Duffy, “An introduction to gradient computation by the discrete adjoint method,” Technical report, Florida State University, Tallahassee (2009).
- Errico, R., 1997. What is an adjoint model? *Bull. Am. Meteorol. Soc.* 78, 2577–2591.
- Giles, M.B., Duta, M.C., Müller, J., Pierce, N.A., 2003. Algorithm developments for discrete adjoint methods. *AIAA J.* 41 (2), 198–205.
- Hu, G., 2018. Adjoint Sensitivity Analysis of the Two-Phase Two-Fluid Model Based on an Approximate Riemann Solver. Ph.D. Dissertation. University of Illinois at Urbana-Champaign.
- Hu, G., Kozlowski, T., 2019. Application of discrete adjoint method to sensitivity and uncertainty analysis in steady-state two-phase flow simulations. *Ann. Nucl. Energy* 126, 122–132.
- Ionescu-Bujor, M., Cacuci, D.G., 2000. Adjoint sensitivity analysis of the RELAP5/MOD3.2 two-fluid thermal-hydraulic code system - II: applications. *Nucl. Sci. Eng.* 136, 85–121.
- Li, S., Petzold, L., 2004. Adjoint sensitivity analysis for time-dependent partial differential equations with adaptive mesh refinement. *J. Comput. Phys.* 198, 310–325.
- C. Lu, Z. Wu, B. Ward, and H. Bindra, “Validation of the 1-D thermal stratification model in gallium environment,” Transactions of the American Nuclear Society, Vol. 122, Virtual Conference, June 8–11, 2020.
- Lu, C., Wu, Z., Wu, X., 2020bb. Enhancing the 1-D SFR thermal stratification model via advanced inverse uncertainty quantification methods. *Nucl. Technol.*
- Lu, C., Wu, Z., Morgan, S., Schneider, J., Anderson, M., Xu, L., Baglietto, E., Bucknor, M., Weathered, M., Bilbao y Leon, S., 2020aa. An efficient 1-D thermal stratification model for pool-type sodium-cooled fast reactors. *Nucl. Technol.*
- Mani, K., Mavriplis, D.J., 2008. Unsteady discrete adjoint formulation for two-dimensional flow problems with deforming meshes. *AIAA J.* 46 (6), 1351–1364.
- Mishra, A., Mani, K., Mavriplis, D., Sitaraman, J., 2015. Time dependent adjoint-based optimization for coupled fluid-structure problems. *J. Comput. Phys.* 292, 253–271.
- S. K. Nadarajah and A. Jameson, “Optimal control of unsteady flows using a time accurate method,” 9th AIAA/ISSMO Symposium on Multidisciplinary Analysis and Optimization Conference, September 4–6, 2002/Atlanta, GA, 2002.
- S. K. Nadarajah, “The discrete adjoint approach to aerodynamic shape,” Dissertation, Stanford University (2003).
- M. Rocklin and E. M. Constantinescu, “Adjoint sensitivity analysis for wind power generation”, University of Chicago as Operator of Argonne National Laboratory (“Argonne”) under Contract No. DEAC02-06CH11357 with the U.S. Department of Energy (2009).
- Rumpfkeil, M.P., Zingg, D.W., 2010. The optimal control of unsteady flows with a discrete adjoint method. *Optimiz. Eng.* 11, 5–22.
- J. Schneider, M. Anerson, E. Baglietto, S. Bilbao y Leon, M. Bucknor, S. Morgan, M. Weathered, L. Xu, “Thermal stratification analysis for sodium fast reactors” proceedings of the international congress on advances in nuclear power plants (ICAPP), Apr. 9–11, 2018 Charlotte, USA.
- Son, S., Lee, J.I., 2018. Application of adjoint sensitivity analysis method to supercritical CO₂ power cycle optimization. *Energy* 147, 1153–1164.
- Thomas, J.P., Dowell, E.H., 2019. Discrete adjoint approach for nonlinear unsteady aeroelastic design optimization. *AIAA J.* 57 (10), 4368–4376.
- Thomas, J.P., Hall, K.C., Dowell, E.H., 2005. Discrete adjoint approach for modeling unsteady aerodynamic design sensitivities. *AIAA J.* 43 (9), 1931–1936.
- B. G. van Bloemen Waanders et al., “Sensitivity technologies for large scale simulation,” Technical report, Sandia national laboratory, SAND2004-6574 (2005).
- Wang, Qiqi, 2013. Forward and adjoint sensitivity computation of chaotic dynamical systems. *J. Comput. Phys.* 235, 1–13. <https://doi.org/10.1016/j.jcp.2012.09.007>.
- Ward, B., Clark, J., Bindra, H., 2019. Thermal stratification in liquid metal pools under influence of penetrating colder jets. *Exp. Therm. Fluid Sci.* 103, 118–125.
- Wu, Z., Lu, C., Morgan, S., Bilbao y Leon, S., Bucknor, M., 2020. A status review on the thermal stratification modeling methods for sodium-cooled fast reactors. *Prog. Nucl. Energy* 125.
- Zahr, M.J., Persson, P.-O., Wilkening, J., 2016. A fully discrete adjoint method for optimization of flow problems on deforming domains with time-periodicity constraints. *Comput. Fluids* 139, 130–147.